Extended states in one-dimensional aperiodic lattices with linearly varying patches

Longyan Gong*

College of Science, Nanjing University of Posts and Telecommunications, Nanjing 210003, China
and Jiangsu Provincial Engineering Research Center of Low-Dimensional Physics and New Energy, Nanjing 210003, China

(Received 5 June 2023; revised 28 August 2023; accepted 24 October 2023; published 14 November 2023)

We introduce a family of one-dimensional aperiodic tight-binding models with linearly varying patches of A-type sites with on-site energies $\epsilon_A = 0$ connected by single B-type sites with $\epsilon_B = W$. We analytically show such structures have strong spatial correlations. We theoretically find states are extended at resonance levels in the vicinity of $E_M^\kappa = -2\cos\frac{\kappa\pi}{M}$ if they are allowed energies, where $M = md$ are the size differences of patches, d is the variation rate of patch sizes, $m \in \mathcal{N}_+$, and $\kappa = 1, 2, \ldots, M-1$. Related delocalization-localization transitions are explored. Numerical evidence is in excellent quantitative agreement with theoretical predictions.

DOI: 10.1103/PhysRevB.108.184201

I. INTRODUCTION

For a long time, the localization phenomenon has attracted a lot of attention in condensed matter physics [1,2]. In uncorrelated disorder potentials, Anderson transitions of noninteracting electrons can happen in 3D systems as potentials increase [3–5]. Such transitions are sometimes referred to as metal-insulator transitions or delocalization-localization transitions. Periodic potentials have translational symmetry, and according to Bloch's theory, all states are extended. In contrast, aperiodic potentials have no translational symmetry but have strong spatial correlations, which is clearly distinguished from the disordered and periodic ones [6]. For instance, states in the Aubry-André-Harper model may be extended, critical, or localized, which depend on potential strength [7,8]. There are extended critical states in the Fibonacci lattices [9] and there may be extended states in the Thue-Morse ones [10,11]. Thus states in aperiodic structures exhibit intermediate properties. In practice, aperiodic structures can provide an inspiring guide to design devices in optoelectronics, optical communication applications, and others [12]. So it is interesting to propose novel aperiodic structures with remarkable properties.

At the same time, it is a challenging and important problem to understand the nature of quantum states [13], i.e., whether states are extended or localized. Disorder can induce localized states and inhibit electronic, vibrational, and transport properties [4]. However, not all states in one-dimensional (1D) disordered systems are localized. For example, multiple-resonance necklace states are typical quasiextended states, which are formed due to the coupling of many nearly degenerate localized states that are centered at different parts of a chain [14,15]. These localized modes are strung together like beads around a necklace, so such states are called necklace states. They can improve the electronic transport properties. A different approach to creating localized states is in periodic systems with a flat-band spectrum [16]. Due to internal symmetries or fine-tuned coupling, flat-band states are perfectly localized to several lattice sites, leading to compact localized states. In such systems, the disorder can induce delocalization, i.e., a transition from an insulating to a metallic phase, dubbed the inverse Anderson transition [17]. More interestingly, resonance nonscattered states have also been found in a 1D random-dimer tight-binding model [18], where A-type and B-type sites are randomly distributed and one component appears in pairs. There are short-range correlations in its on-site potentials. Since then, resonance states have been found in similar models, for instance, random trimer [19], random dimer-trimer [20], and random n-mer ones [21–23].

Recently, Bykov *et al.* proposed guided-mode resonant gratings with linearly varying periods [24]. These structures can exhibit resonance reflectance peaks with the spatial position depending on the incident wavelength, so such gratings can be used as novel optical filters. It is worth extending it to other fields. Very recently, Citrin proposed quadratic superlattices and found extended states [25]. In fact, it is a specific linearly-varying-period structure. However, the mechanism of the presence of extended states should be further explained.

Inspired by the above mentioned, we propose a family of 1D aperiodic lattices with linearly varying periods. We analytically show such structures have strong spatial correlations. With a tight-binding model, we theoretically find extended states at resonance energies and their underlying mechanism. The state localization properties are also intensively certified by numerical evidence.

II. MODEL

The family of 1D aperiodic structure is sketched in Fig. 1, where the distance between two nearest sites is set to the unit. The jth patch has $s_j = d_0 + (j-1)d$ A-type sites, and we call it an s_j-mer. Here, d_0 is the size of the first patch, d is the variation rate of patch sizes, and $j = 1, 2, \ldots, j_m$. They are linearly varying patches (LVPs) [24]. The inlaid single B-type sites link these LVPs with positions $Z_j = j(j+$

*lygong@njupt.edu.cn

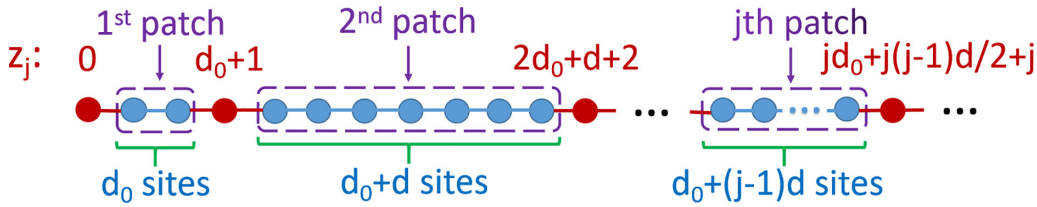

FIG. 1. Schematic diagram of 1D aperiodic lattices. The jth linearly varying patch has $s_j = d_0 + (j-1)d$ A-type sites (blue solid circles), where d_0 is the size of the first patch and d is the variation rate of patch sizes; the inlaid single B-type sites (red solid circles) link these patches with positions $Z_j = jd_0 + j(j-1)d/2 + j$. Here, $d_0 = 2$ and $d = 5$ are given as examples.

$1)d/2 + j$. The basic length d defines a family of structures. The structure is periodical if $d = 0$. It becomes the model proposed in Ref. [25] if $d_0 = 0$ and $d = 2$. Further, these s_j-mers are arranged in order of increasing size and there are long-range correlations in structures (see the next section), which is different from those in the random-dimer model [18] as well as its variants [19–23] having short-range correlations.

For an electron moving in such structures, the nearest-neighbor tight-binding Hamiltonian can be written as

$$H = \sum_{n=0}^{N-1} \varepsilon_n |n\rangle\langle n| - t \sum_{n=0}^{N-2} (|n\rangle\langle n+1| + |n+1\rangle\langle n|), \quad (1)$$

where $|n\rangle = c^\dagger|0\rangle$, $c^\dagger$ is the creation operator, ε_n is the on-site potential, and t is the nearest-neighbor hopping integral. The system size $N = Z_{j_m} + 1$. In Fig. 1, for simplicity, we suppose the A-type sites have zero potentials and the B-type sites have constant potentials with strength W, i.e.,

$$\varepsilon_n = \begin{cases} W, & n = Z_j \text{ and } j = 0, 1, 2, \ldots, j_m, \\ 0, & \text{otherwise.} \end{cases} \quad (2)$$

At $W = 0$, eigenstates can be expressed by $|\Psi_\beta\rangle = \sum_{n=0}^{N-1} \psi_\beta(n)|n\rangle = \sum_{n=0}^{N-1} \sqrt{\frac{2}{N+1}} \sin[\frac{\beta(n+1)\pi}{N+1}]|n\rangle$ with $\beta = 1, 2, \ldots, N$, where all states are extended [26,27].

III. RESULTS

We will study structure factors of the 1D aperiodic lattices shown in Fig. 1, energy spectrum properties of the Hamiltonian in Eq. (1), state localization properties, and the effect of randomness. In the following, results for $d = 5$ along with $d_0 = 2$ are presented.

A. Structure factors

For the structure in Fig. 1, structure factors are defined by

$$S(k) = \left| \sum_{j=0}^{j_m} \exp(ikZ_j) \right|^2, \quad (3)$$

where k are wave vectors and $i = \sqrt{-1}$. They directly relate to the results of x-ray and neutron-diffraction experiments [6,12]. They also underlie behaviors observed in the electronic, vibrational, and transport properties. We set $k = \frac{2}{L}\widetilde{k}\pi$, where L is an integer and $\widetilde{k} = 1, 2, \ldots, [L/2]$. At $L = 7$, 9, 11, and 13, we get

$$S(k) = S_L j_m^\alpha, \quad (4)$$

where $S_7 = 1/7$, $S_{11} = 1/11$, and $S_{13} = 1/13$; $S_9 = 1/3$ at $\widetilde{k} = 3$, and $S_9 = 1/9$ at $\widetilde{k} = 1, 2$ and 4, respectively; and the scaling exponent $\alpha = 2$ (see Appendix A). They agree with the numerical results plotted in Figs. 2(a) and 2(b). Like quasiperiodic systems [28,29], we find there are sequences of hierarchical δ-function peaks in $S(k)$; i.e., for some k, the factor S_L is finite even at system sizes $N \to \infty$. In Ref. [25], it is found $\alpha \to 2$ as $k \to 0$ at $d = 2$ and $d_0 = 0$, which agrees with our results. The exponent $\alpha = 2$ has been found in periodic and some quasiperiodic structures [30]. So it indicates that the structure in Fig. 1 is aperiodic, with strong spatial correlations. They may induce extended or critical states.

B. Resonance levels

If we only consider two patches, with the theory of a trace map of transfer matrices [31], we analytically show at energies

$$E_M^\kappa = -2\cos\frac{\kappa\pi}{M} \quad (5)$$

the trace of transfer matrices $|\chi| \leqslant 2$ and corresponding states are extended or critical, where M is the size difference of the two patches, and $\kappa = 1, 2, \ldots, M-1$ (see Appendix B). For a string with more than two patches, using a numerically accurate renormalization scheme [32], both the sites in intermediate patches and intermediate inlaid sites can be renormalized into "one" inlaid site, so they can be taken as "two patches." The expression of E_M^κ in Eq. (5) also holds but M is the size difference of the patches at two edges. This is a local heuristic argument. The details are given in Appendix B. However, for a string with many patches, the renormalized "one" inlaid site may induce localization effects.

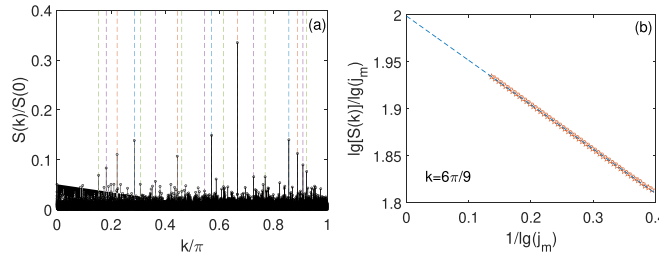

FIG. 2. (a) Structure factors $S(k)$ versus wave vectors k at system size $N = 107\,227$ ($j_m = 207$). (b) Finite-size scaling of $S(k)$ at $k = 6\pi/9$. In (a), the vertical dashed lines correspond to $k = \frac{2}{L}\widetilde{k}\pi$ with $\widetilde{k} = 1, 2, \ldots, [L/2]$, and $L = 7$ (blue), 9 (green), 11 (red), and 13 (purple), respectively. In (b), the dashed line is linearly fitted to corresponding data.

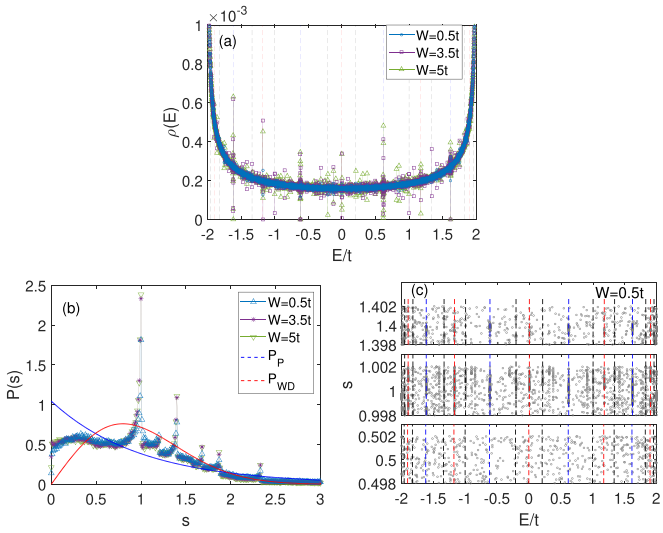

FIG. 3. (a) Density of state versus energies E and (b) level spacing distributions $P(s)$, where $W = 0.5t$, $3.5t$, and $5t$, and system size $N = 301\,197$ ($j_m = 347$). (c) Level spacings s versus E at $W = 0.5t$. The vertical dashed lines in (a) and (c) are for energies E_M^κ with $M = 5$ (blue), $M = 10$ (red), and $M = 15$ (black), respectively. In (b), P_P and P_{WD} are for Poisson and Wigner-Dyson distributions, respectively.

For a few patches (superpatches), there are states with energies E_M^κ. Locally, these states are extended in a few patches; globally, they are localized in different spaces of the whole lattices. So they are locally extended localized states. In our model (Fig. 1), these patches linearly vary with variation rate d. Such locally extended localized states with the same energies E_M^κ exist for each superpatch, i.e., resonance conditions, where $M = md$ and $m \in \mathcal{N}_+$. When these superpatches are linked together by inlaid B-type sites, the energies of whole lattices around E_M^κ may become resonance levels if they are allowed energies, and related states may be extended.

C. Energy spectrum properties

Statistical properties of the energy spectrum can reflect overall properties of systems [5,33–35]. Two quantities are of special interest, i.e., the density of states (DOS) and level spacing distributions.

The singularity of the DOS can reflect mobility edges in quasiperiodic systems [36] and resonance energies in quantum percolation models [37]. In Fig. 3(a), we plot the DOS $\rho(E)$, which is defined by $\rho(E) = \sum_{\beta=1}^{N} \delta(E - E_\beta)$ and E_β is the βth eigenenergy. We only consider energies $|E| \leqslant 2$. When E is beyond this range, we find states are localized. Figure 3(a) shows in the curves of the $\rho(E)$ there are many sharp peaks along with sharp dips, i.e., the singularity in DOS. The sharp dips mean there may exist energy gaps. Interestingly, most of these peaks (dips) in the DOS present at energies that are around E_M^κ with $M = 5, 10$, and 15, which are labeled by vertical dashed lines. The three Ms are the size difference between nearest-neighbor (NN), next NN, and next to next NN patches. In the figure, the $\kappa = 1, 2, 3, 4$ for $M = 5$, $\kappa = 1, 3, 5, 7, 9$ for $M = 10$, and $\kappa = 1, 2, 4, 5, 7, 8, 10, 11, 13, 14$ for $M = 15$. This can ensure the repeated energies are taken into account only once. For aperiodic systems, such singularities may indicate there exist critical or extended states [36].

At the same time, for 3D Anderson models, level spacing distributions $P(s)$ are the Wigner-Dyson distribution P_{WD} in a metal region, obey the Poisson law P_P in an insulator region, and they are intermediate at the metal-insulator transitions [38], where s are spacings between unfolded nearest-neighboring levels. The $P(s)$ are also intermediate distributions in disorder systems with long-range correlations [39] and in quasiperiodic systems such as Fibonacci and Thue-Morse chains [34]. We plot $P(s)$ in Fig. 3(b) for $W = 0.5t$, $3.5t$, and $5t$, respectively. It shows the behaviors of $P(s)$ are intermediate between P_{WD} and P_P. Such behaviors are consistent with that the structures in Fig. 1 are aperiodic. Further, Fig. 3(b) shows $P(s)$ have local sharp peaks at some of s. In Fig. 3(c), we show the two main peaks at $s = 1$ and 1.4 are mainly attributed to these energies with singularity in DOS. As a comparison, at $s = 0.5$ [without peaks in $P(s)$], their attributions are common.

D. State localization properties

We use three effective quantities, i.e., the local tensions [40,41], Lyapunov exponents [32], and fractional dimensions [5], to directly characterize state localization properties.

1. Local tension

First, the local tension successfully distinguishes metals from insulators in many-body systems [40]. For 1D systems, it is defined by $\lambda_{xx}^2 = \langle\Psi|\hat{Q}_x^\dagger\hat{Q}_x|\Psi\rangle - \langle\Psi|\hat{Q}_x^\dagger|\Psi\rangle\langle\Psi|\hat{Q}_x|\Psi\rangle$, where $\hat{Q}_x = \frac{N}{2\pi i}\sum_{n=0}^{N-1}[\exp(\frac{2\pi i}{N}\hat{x}_n) - 1]$, and $\hat{x}_n$ is the position operator in the x direction [42], i.e., $\hat{x}_n = |n\rangle$. The reduced local tension (RLT) is defined by

$$\Lambda = 2\pi\lambda_{xx}/N. \tag{6}$$

As system sizes $N \to \infty$, $\Lambda \to 1$ for extended states and $\Lambda \to 0$ for localized ones [43].

Figure 4(a) shows generally the Λ are relatively large (small) for relative small (large) W. The vertical dashed lines mark the position of E_M^κ obtained from Eq. (5). The Λ are relatively large when E are around these E_M^κ [also seen Fig. 4(b)], which means these states may be extended. Partial enlargers of Fig. 4(a) for E near four E_M^κ are plotted in Fig. 4(c). It shows when W are relative large, energy gaps along with level squeezing will occur, which corresponds to the singularity in DOS shown in Fig. 3(a); for these squeezed levels, the values of Λ may be relatively large; in these energy gaps, states with energies E_M^κ are not permitted. In Fig. 4(d), we plot typical wave functions with E that are nearest to three E_M^κ, where they spread over the whole lattices; i.e., they are extended states. In fact, we find the same results for other cases, including different d_0 at $d = 5$ and other ds (see Appendix C).

Figures 5(a)–5(c) show at $W = 0.5t$, as system sizes N increase, the values of Λ are close to 1 for states at energies $E_M^\kappa = E_5^3, E_{10}^5$, and E_{15}^{10}, respectively, while they decrease when states with energies E depart from these E_M^κ. In Fig. 5(d), we plot the Λ versus E_M^κ with $M = 300$. In calculations, these states are the ones with energies nearest to E_M^κ. It shows most of Λ almost equal 1, which correspond

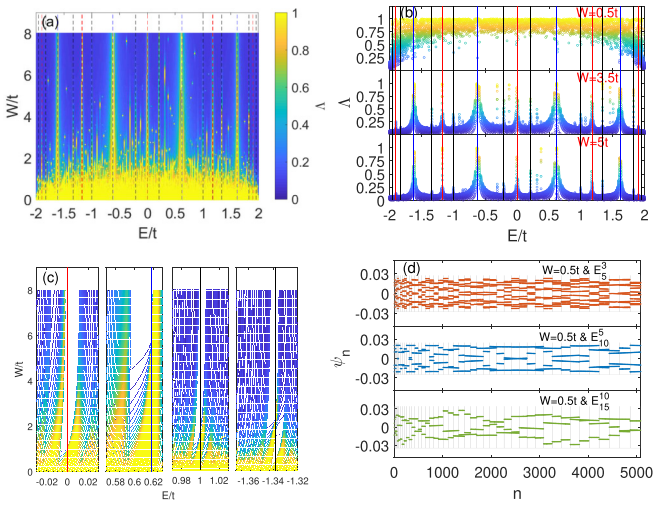

FIG. 4. (a) RLTs Λ as functions of energies E and potential strengths W. (b) The Λ versus E at $W = 0.5t, 3.5t$, and $5t$, respectively. (c) From left to right, partial enlarger for E near $E^5_{10} = 0$, $E^3_5 \approx 0.618t$, $E^{10}_{15} = t$, and $E^4_{15} \approx -1.338t$, respectively. (d) At $W = 0.5t$, three typical wave functions with eigenenergies nearest to E^3_5, E^5_{10}, and E^{10}_{15}, respectively. The vertical dashed lines in [(a)–(c)] are the same in Fig. 3. The gray fold lines in (d) are for the functions of on-site potentials. System size $N = 5086$ ($j_m = 45$).

to extended states; many are much smaller than 1, which correspond to localized states. As a comparison, we also plot the Λ at $M = 301$. The value 301 is not the size difference of patches, so the corresponding E^κ_M are not resonance energies. For them, Fig. 5(d) shows almost all Λ are smaller than 1, which means these states are localized.

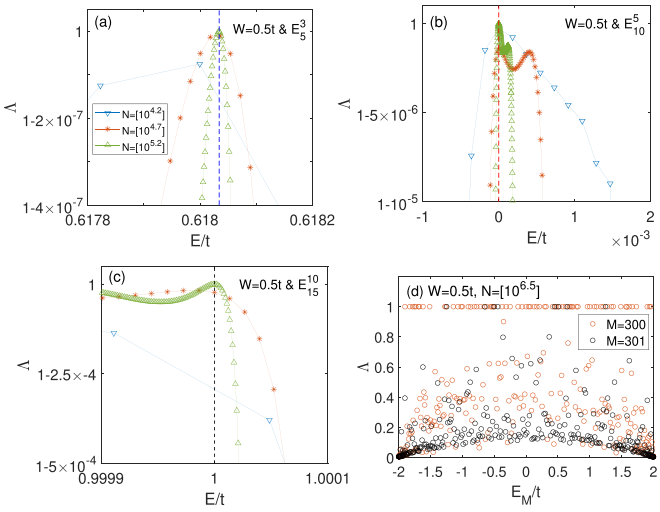

FIG. 5. At $W = 0.5t$, RLTs Λ as functions of energies E when they are near (a) E^3_5, (b) E^5_{10}, and (c) E^{10}_{15}, respectively. (d) The Λ versus E^κ_M with $M = 300$ and 301. The vertical dashed lines in [(a)–(c)] are the same in Fig. 3. System sizes $N = [10^{4.5}] = 31\,980$ ($j_m = 227$), $[10^{5.5}] = 317\,019$ ($j_m = 356$), and $[10^{6.5}] = 3\,164\,626$ ($j_m = 1125$). Here, $[10^z]$ denotes the system size that is greater than and nearest to 10^z.

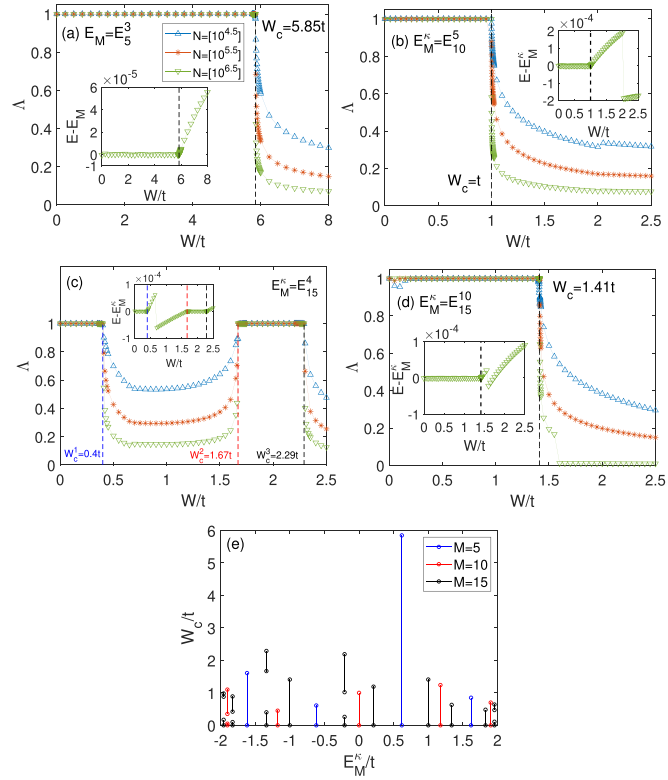

FIG. 6. RLTs Λ as functions of potential strengths W at energies E that are nearest to (a) E^3_5, (b) E^5_{10}, (c) E^4_{15}, and (d) E^{10}_{15}, respectively. (e) W_c versus E^κ_M at $M = 5, 10$, and 15, and lines represent the range of W where states are extended. The insets in [(a)–(d)] show the $E - E^\kappa_M$ versus W at $N = [10^{6.5}]$. The vertical dashed lines in [(a)–(d)] mark the position of W_c.

In Fig. 6, we plot the Λ as functions of W when E are nearest to E^κ_M. It shows the values of Λ are close to 1 in some regions of W, where states are extended. We call them "extended-state-W regions." And Λ rapidly decrease at the boundaries of such regions. These are the signatures of delocalization-localization transitions, and the corresponding critical potential strength is denoted by W_c. So the states have delocalization-localization transitions at W_c. We plot the $E - E_M$ versus W in the insets of Figs. 6(a)–6(d) at $N = [10^{6.5}]$. We find in extended-state-W regions, $E - E^\kappa_M \approx 0$; i.e., E^κ_M is allowed energies of systems. In localized state regions of W, $E - E^\kappa_M$ are relatively large; as displayed in Fig. 4(c), these E^κ_M are in energy gaps. We plot the phase diagram in Fig. 6(e) for $M = 5, 10$, and 15, where lines represent the ranges of extended-state-W regions. Similarly, we can obtain phase diagrams for larger M, but the corresponding ranges are relative small, or even disappear.

2. *Lyapunov exponent*

Second, the energy-dependent Lyapunov exponent (LE) $\gamma(E)$ is another often used quantity to characterize electronic localization properties, which is defined by

$$\gamma(E) = -\lim_{N\to\infty}\left[\frac{1}{N}\ln\left|\frac{G_{NN}(E)}{G_{1N}(E)}\right|\right], \tag{7}$$

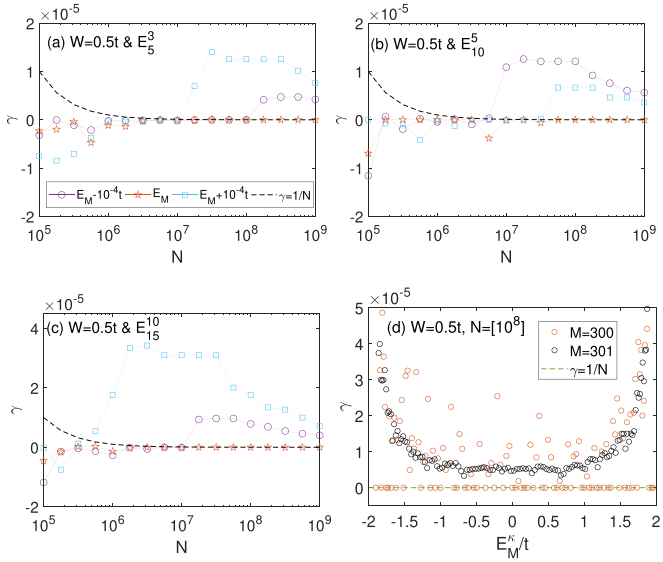

FIG. 7. At $W = 0.5t$, LEs γ versus system sizes N with energies E at and near (a) E_5^3, (b) E_{10}^5, and (c) E_{15}^{10}, respectively. The γ versus E_M^κ with $M = 300$ and 301. The dashed curves in [(a)–(d)] are for the function $\gamma = 1/N$.

where $G_{NN}(E)$ and $G_{1N}(E)$ are the Green-function matrix elements. We use a numerically accurate renormalization scheme to calculate them [32]. Generally, the LE γ is inversely proportional to localization length. At finite system sizes for extended states, γ may be less than zero. In practice, for finite system size the inequality $\gamma \leqslant 1/N$ is often used as a sign that states are extended.

Figures 7(a)–7(c) show $\gamma \leqslant 1/N$ when energies at E_M^κ; as system sizes N are large enough, $\gamma > 1/N$ when energies deviate from E_M^κ even a little bit. This implies E_M^κ are discrete resonance levels. In Fig. 7(d), we plot the γ versus E_M^κ with $M = 300$. It shows most of γ are smaller than $1/N$, which indicates these states are extended. At the same time, many are larger than $1/N$. We also plot the γ at $M = 301$. Conversely, all values of γ are larger than $1/N$; i.e., all these states are localized ones.

Panels (a), (c), (e), and (g) of Fig. 8 show as N increases, there exist regions that $\gamma \to 0$ and γ are finite. The W_c separates the two types of regions, which agrees with that shown in Fig. 6. At the same time, panels (b), (d), (f), and (h) of Fig. 8 plot γ versus W at E_M^κ and $E_M^\kappa \pm 10^{-4}t$. They show in extended-state-W regions, when energies deviate from E_M^κ a little bit, γ are finite, which means these states are localized.

Figures 9(a)–9(d) show the behavior of the γ with respect to system sizes N when potential strength is at W_c, $W_c - 0.1t$, $W_c + 0.01t$, and $W_c + 0.5t$, respectively. As the logarithm is applied, the γ for some N are not displayed if their values are smaller than zero. These figures show when W are in the extended-state-W regions, generally, $\gamma \propto N^{-1}$, which confirms these states are extended. At the same time, when W are beyond such regions, $\gamma \propto N^{-\nu}$ and scaling exponents ν are less than 1, which indicates these states are localized. To demonstrate the localization properties intuitively, we plot typical wave functions with eigenenergies nearest to E_5^3 in Fig. 10. We find the state in Fig. 10(a) is an extended state,

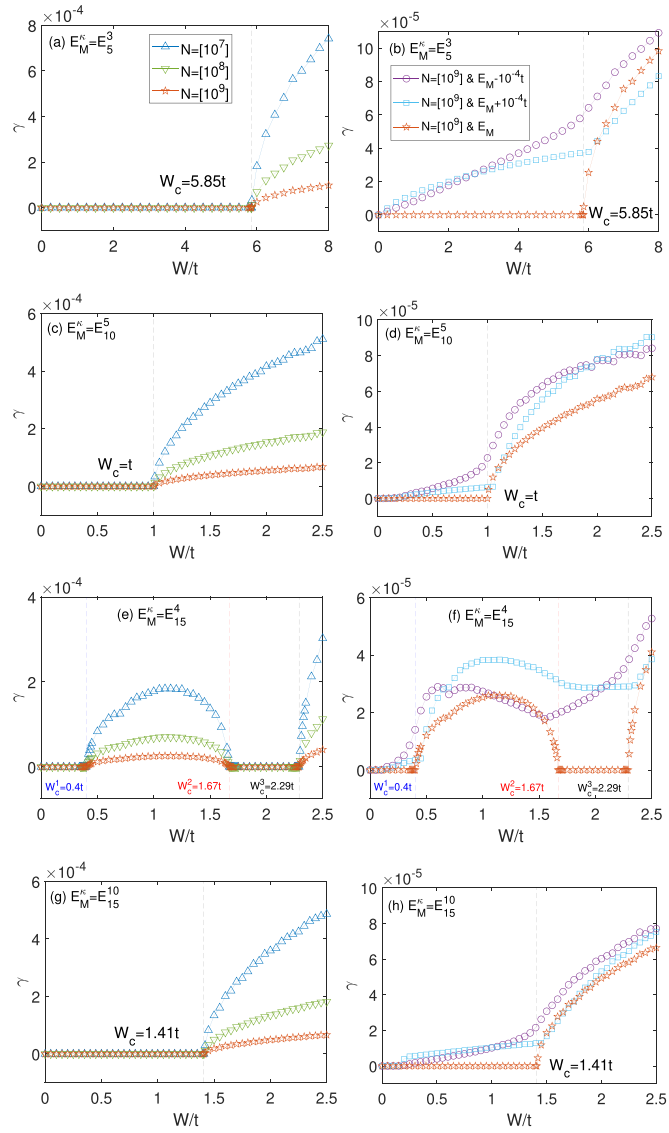

FIG. 8. LEs γ as functions of potential strength W for energies E at and near (a), (b) E_5^3; (c), (d) E_{10}^5; (e), (f) E_{15}^4; and (g), (h) E_{15}^{10}, respectively. The vertical dashed lines in [(a)–(d)] mark the position of W_c.

which spreads over the whole lattices. The states in Figs. 10(b) and 10(d) are critical (intermediate) and localized ones, respectively. In Fig. 10(c), the varying of the state (with W being close to W_c) is similar as that in Fig. 10(b). From Fig. 9(a), we can infer such state should be localized for the corresponding ν much less than 1 when N is large enough. At the same time, for critical and localized states, the square moduli of wave functions are plotted in Figs. 10(e) and 10(f), which exhibit three hierarchies and may indicate such wave functions have fractal properties. Interestingly, every hierarchy can be fitted by the function $y = ax^{b_1} \exp(-cx^{b_2})$. In 1D systems, for exponentially localized states [44], LEs γ remain finite when $N \to \infty$, so $\nu = 0$; for power-law localized states [45], $\gamma \to 0$ as $N \to \infty$, but ν are finite. Different from the two cases, in the present work, critical and localized states can be described by the power-law function tuned with exponential decay functions. Lyapunov exponents can also be

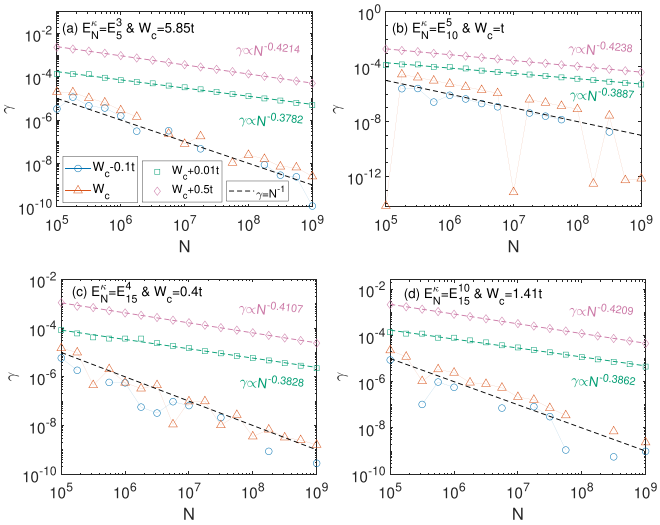

FIG. 9. LEs γ versus system sizes N with potential strength at critical W_c, $W_c - 0.1t$, $W_c + 0.01t$, and $W_c + 0.5t$, respectively. Energies E are at (a) E_5^3, (b) E_{10}^5, (c) E_{15}^4, and (d) E_{15}^{10}, respectively, where the dashed lines are for the function $\gamma \propto N^{-\nu}$.

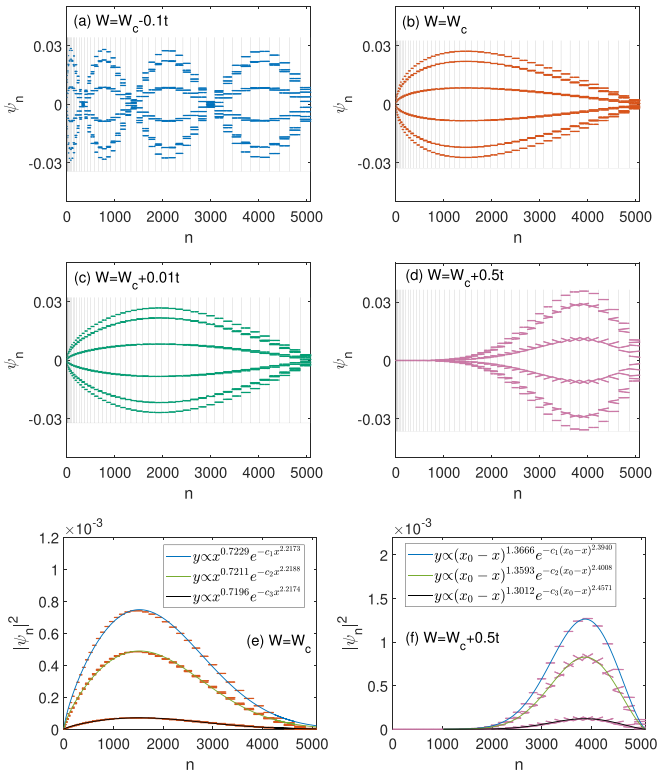

FIG. 10. Typical wave functions with eigenenergies nearest to E_5^3 when W equals (a) $W_c - 0.1t$, (b) W_c, (c) $W_c + 0.01t$, and (d) $W_c + 0.5t$, respectively, where $W_c = 5.85t$. The square moduli of wave functions when (e) $W = W_c$ and (f) $W = W_c + 0.5t$. The gray fold lines in [(a)–(d)] are for the functions of on-site potentials. In (e), $c_1 = 2.8712 \times 10^{-8}$, $c_2 = 2.8321 \times 10^{-8}$, and $c_3 = 2.8578 \times 10^{-8}$. In (f), $c_1 = 2.3522 \times 10^{-8}$, $c_2 = 2.2195 \times 10^{-8}$, and $c_3 = 1.3897 \times 10^{-8}$ and $x_0 = 5087$. System size $N = 5086$ ($j_m = 45$).

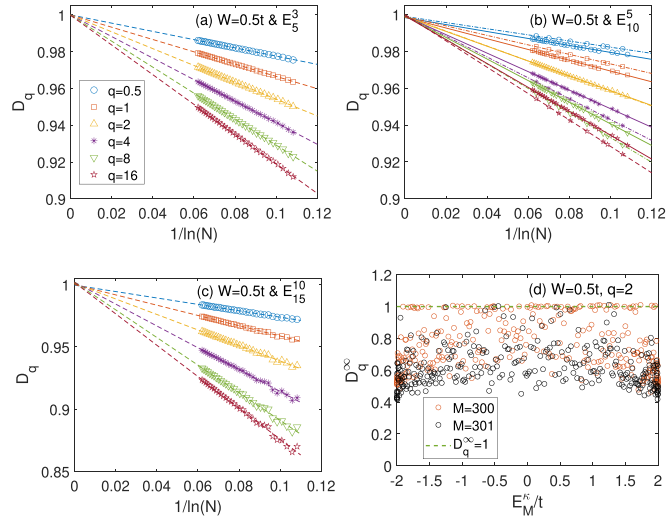

FIG. 11. At $W = 0.5t$, FDs D_q versus $1/\ln(N)$ for energies E that are nearest to (a) E_5^3, (b) E_{10}^5, and (c) E_{15}^{10}, respectively. (d) At $q = 2$, the D_q^∞ versus E_M^κ with $M = 300$ and 301. The dashed lines in [(a)–(c)] are linearly fitted to corresponding data. In (a), there are two branches in the curves of D_q versus $1/\ln(N)$.

calculated by [45] $\gamma = \frac{1}{2N}\sum_{x=1}^{N} \ln \frac{y(x)}{y(x-1)}$, so it can be written as $\gamma = \gamma_{\text{power}} + \gamma_{\text{exp}}$. As N increase, the former determines the scaling property of γ, and the latter determines the upper bound of γ. This agrees with that shown in Fig. 9, where the scaling exponents ν are close to 1 for critical states and they are much less than 1 for localized states.

3. Fractional dimension

Third, do these resonance states remain extended in the thermodynamic limit? We shed light on this problem with the fractional dimension (FD) [5], which is defined by $D_q = \frac{1}{1-q}\ln I_q/\ln(N)$, where $I_q = \sum_{n=0}^{N} |\psi_\beta(n)|^{2q}$ and q is the moment. In the thermodynamic limit,

$$D_q^\infty = \lim_{N\to\infty} D_q. \tag{8}$$

In 1D systems, $D_q^\infty = 1$ for perfectly extended states, $D_q^\infty = 0$ for localized states, and $0 < D_q^\infty < 1$ for intermediate ones [5,46].

At $W = 0.5t$, Figs. 11(a)–11(c) show D_q linearly decrease with $1/\ln(N)$. When $N \to \infty$, $D_q^\infty \approx 1$, which indicates these states are extended. For $M = 300$ and 301, at $q = 2$, the D_q^∞ versus E_M^κ are plotted in Fig. 11(d). It shows for $M = 300$, most of D_q^∞ almost equal 1, which indicates these states are extended. At the same time, many are smaller than 1. In contrast, for $M = 301$, almost all D_q^∞ are smaller than 1; i.e., they are localized ones.

Figure 12 displays the variations of D_q^∞ with W. It shows for the four E_M^κ, there exist regions that $D_q^\infty \approx 1$ and $D_q^\infty < 1$. The W_c separates the two types of regions, which agrees with that shown in Fig. 6 and Fig. 8.

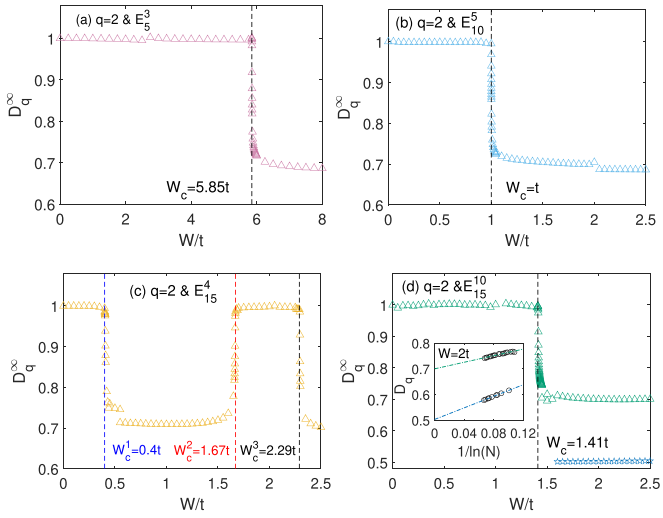

FIG. 12. At $q = 2$, FDs D_q^∞ as functions of potential strength W for energies E that are nearest to (a) E_5^3, (b) E_{10}^5, (c) E_{15}^4, and (d) E_{15}^{10}, respectively. The vertical dashed lines in [(a)–(d)] mark the position of W_c. The inset in (c) shows D_q versus $1/\ln(N)$ at $W = 2t$, where there are two branches in the curve of D_q versus $1/\ln(N)$.

E. Effect of randomness

Three kinds of randomness are considered, i.e., disordered on-site potentials, randomly arranged patches, and fluctuations in patch sizes.

1. Disordered on-site potentials

For the kind of randomness, the on-site potential for B-type sites in Eq. (2) becomes $\varepsilon_n = W(1 + f_\varepsilon \xi_n)$, where ξ_n is a random variable uniformly chosen within the range $[-1/2, 1/2]$ and f_ε characterizes the degree of randomness. The patch sizes and their arrangement in space are the same as that in Fig. 1.

In Fig. 13(a), we plot RLTs Λ versus energies E for $f_\varepsilon = 0.5$, where $W = 2t$ is as an example. By contrast, we also plot Λ for $f_\varepsilon = 0$. We find Λ will decrease when randomness is present; i.e., disorder can induce localization. However, Λ are relatively large when E are around E_M^κ, which means these states are more extended than other states. Figures 13(b) and 13(c) show the larger the randomness is, the smaller the Λ is; in general, when randomness is present, Λ are relative large in extended-state-W regions [randomness vanishes; see Fig. 6(e), the same below].

2. Randomly arranged patches

As mentioned in Sec. II, the jth patch in Fig. 1 has $s_j = d_0 + (j-1)d$ A-type sites, i.e., the s_j-mer, where $j = 0, 1, \ldots, j_m$. These mers are arranged in order of increasing size. We refer to it as the ordered lattice. In the random-dimer model [18] as well as its variants [19–23], the dimer, trimer, dimer-trimer, and n-mer are present randomly in space. Similarly, we can randomly shuffle all the patches, i.e., $\{s_j$-mer$\}$, in space. We call it the shuffled lattice. For this kind of randomness, the on-site potentials ε_n do not change, which are chosen according to Eq. (2).

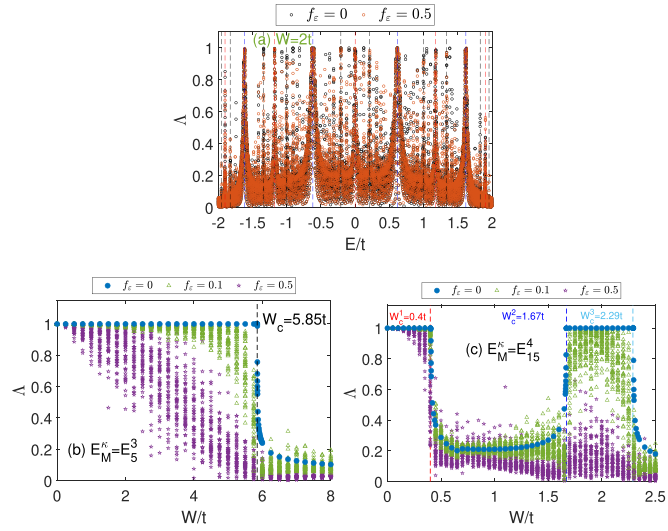

FIG. 13. (a) RLTs Λ as functions of energies E at $W = 2t$. The Λ as functions of potential strengths W at energies E that are nearest to (b) E_5^3 and (c) E_{15}^4, respectively, where results of 50 random realizations of $\{\varepsilon_n\}$ are given for each W. The vertical dashed lines in (a) are the same in Fig. 3. The vertical dashed lines in (b) and (c) mark the position of W_c for $f_\varepsilon = 0$. System size $N = 10\,273$ ($j_m = 64$) for (a), and $N = [10^6] = 1\,002\,040$ ($j_m = 633$) for (b) and (c).

In Fig. 14(a), we plot the Λ versus energies E for the shuffled lattices at $W = 2t$. Compared to that for the ordered ones, Λ almost does not change when E are around E_5^3 and it rapidly decreases at other E_M^κ. For E_5^3, Fig. 14(b) shows Λ almost equal to 1 in the extended-state-W region, which means these states are extended. In fact, we can get similar

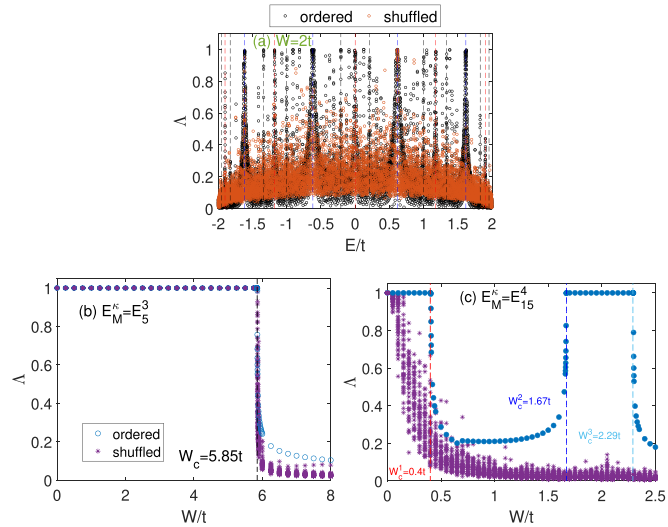

FIG. 14. (a) RLTs Λ as functions of energies E at $W = 2t$. The Λ as functions of potential strengths W at energies E that are nearest to (b) E_5^3 and (c) E_{15}^4, respectively, where results of 50 random realizations of $\{\varepsilon_n\}$ are given for each W. The vertical dashed lines in (a) are the same in Fig. 3. The vertical dashed lines in (b) and (c) mark the position of W_c for the ordered case. System size $N = 10\,273$ ($j_m = 64$) for (a), and $N = [10^6] = 1\,002\,040$ ($j_m = 633$) for (b) and (c).

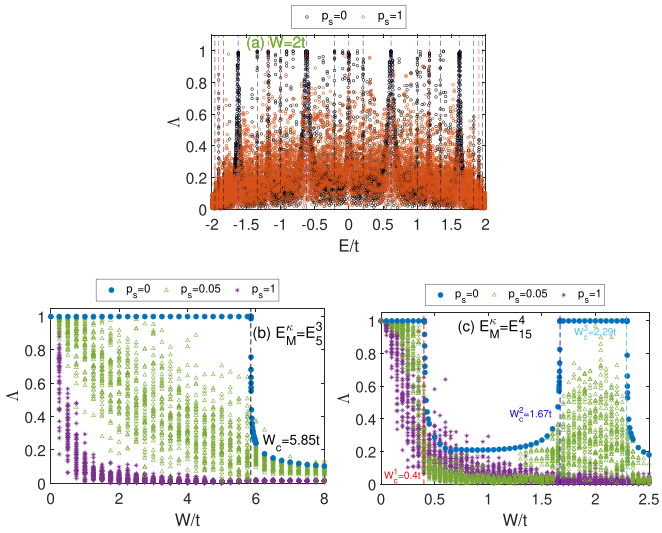

FIG. 15. (a) RLTs Λ as functions of energies E at $W = 2t$. The Λ as functions of potential strengths W at energies E that are nearest to (b) E_5^3 and (c) E_{15}^4, respectively, where results of 50 random realizations of $\{\varepsilon_n\}$ are given for each W. The vertical dashed lines in (a) are the same in Fig. 3. The vertical dashed lines in (b) and (c) mark the position of W_c for $p_s = 0$. At $p_s = 0$, system size $N = 10\,273$ ($j_m = 64$) for (a), and $N = [10^6] = 1\,002\,040$ ($j_m = 633$) for (b) and (c); at $p_s = 0.05$ and 1, system sizes approach to just mentioned Ns, respectively.

results for other E_5^κ ($\kappa = 1, 2$, and 4). For other E_M^κ ($M = 10, 15, \ldots$), the same as shown in Fig. 14(c); Λ heavily decrease even in extended-state-W regions when randomness is present; i.e., extended states will disappear except at $W = 0$. We know for the shuffled lattices, the size difference between nearest-neighbor patches will be $M' = 5m'$ and m' may be $1, 2, \ldots$. As mentioned in Sec. III B, the corresponding locally extended localized states have the energies $E_{M'}^{\kappa'} = -2\cos\frac{\kappa'\pi}{5m'}$, i.e., Eq. (5). For each patch, there always exists κ' satisfying $E_{M'}^{\kappa'} = E_5^\kappa$ (resonance conditions). So these states with energies E_5^κ can be merged together to form extended states. However, if $M = 10, 15, \ldots$, the relation that $E_{M'}^{\kappa'} = E_M^\kappa$ is not always satisfied, so states with these E_M^κ ($M > 5$) are localized ones.

3. *Fluctuations in patch sizes*

Another randomness is that there are small fluctuations in patch sizes s_j in Fig. 1. For the randomness, we consider $s_j = d_0 + (j-1)d + [\Delta_s\eta_j]$ with probability p_s, and $s_j = d_0 + (j-1)d$ with probability $1 - p_s$, where $[Z]$ represents the integer of Z, and η_j is a random variable uniformly chosen within the range $[-1/2, 1/2]$. For this kind of randomness, we do not alter the on-site potential ε_n in Eq. (2).

In Fig. 15(a), when $W = 2t$, we plot the Λ versus energies E. We take $\Delta_s = 5$ as an example. Comparing with that for $p_s = 0$, we find Λ will decrease for $p_s = 1$. The Λ as functions of potential strengths W are plotted in Figs. 15(b) and 15(c) at energies E that are nearest to E_5^3 and E_{15}^4, respectively. They show Λ become smaller as randomness is present, which means there are absences of extended states. Resonance conditions cannot be satisfied for patches with size fluctuations, so all states are localized except at $W = 0$.

IV. CONCLUSIONS

A family of 1D aperiodic lattices with linearly varying patches is introduced. Analytically, structure factors show these lattices have strong spatial correlations. In the frame of nearest-neighbor tight-binding models, we show extended states at resonance levels. Three quantities, i.e., local tensions, Lyapunov exponents, and fractional dimensions, all can certify the nature of these extended states. These studies may be useful to design high-quality one-frequency selection devices in optoelectronics, optical communication applications, and other fields.

ACKNOWLEDGMENTS

The author would like to thank Hongli Zeng and Yaoxian Zheng for fruitful discussions and useful comments. This work was supported by the National Natural Science Foundation of China (Grant No. 62375140).

APPENDIX A: SCALING LAWS OF STRUCTURE FACTORS

In Fig. 1, the position of inlaid B-type site $Z_j = jd_0 + j(j-1)d/2 + j$ with $j = 0, 1, 2, \ldots, j_m$. When $d_0 = 2$ and $d = 5$,

$$Z_j = \frac{5j^2 + j}{2}. \tag{A1}$$

We set $k = \frac{2}{L}\widetilde{k}\pi$ and $\widetilde{Z}_j^L = \frac{5j^2+j}{L}$, where L is an integer and $\widetilde{k} = 1, 2, \ldots, [L/2]$. Then

$$kZ_j = \widetilde{k}\pi\widetilde{Z}_j^L. \tag{A2}$$

We represent $j = Lj_0 + \ell$ with $\ell = 0, 1, \ldots, L-1$. At $L = 7, 9, 11$, and 13, the values of mod $(\widetilde{Z}_j^L, 2)$ are listed in Table I.

TABLE I. Values of mod $(\widetilde{Z}_j^L, 2)$.

	mod $(\widetilde{Z}_j^L, 2)$			
ℓ	$L = 7$	$L = 9$	$L = 11$	$L = 13$
0	0	0	0	0
1	6/7	2/3	6/11	6/13
2	8/7	4/9	0	22/13
3	6/7	4/3	4/11	22/13
4	0	4/3	18/11	6/13
5	4/7	4/9	20/11	0
6	4/7	2/3	10/11	4/13
7		0	10/11	18/13
8		4/9	20/11	16/13
9			18/11	24/13
10			4/11	16/13
11				18/13
12				4/13

Based on mod $(\widetilde{Z}_j^L, 2)$ and the definition of the structure factor in Eq. (3), at $j_m \to \infty$, we get

$$S(k) = S_L j_m^2, \tag{A3}$$

i.e., the scaling parameter $\alpha = 2$, where

$$S_7 = \left|\frac{1}{7}\left\{2 + 2\exp\left(i\frac{4}{7}\widetilde{k}\pi\right) + 2\exp\left(i\frac{6}{7}\widetilde{k}\pi\right) + \exp\left(i\frac{8}{7}\widetilde{k}\pi\right)\right\}\right|^2, \tag{A4}$$

$$S_9 = \left|\frac{1}{9}\left\{2 + 2\exp\left(i\frac{2}{3}\widetilde{k}\pi\right) + 2\exp\left(i\frac{4}{3}\widetilde{k}\pi\right) + 3\exp\left(i\frac{4}{9}\widetilde{k}\pi\right)\right\}\right|^2, \tag{A5}$$

$$S_{11} = \left|\frac{1}{11}\left\{2 + 2\exp\left(i\frac{4}{11}\widetilde{k}\pi\right) + \exp\left(i\frac{6}{11}\widetilde{k}\pi\right) + 2\exp\left(i\frac{10}{11}\widetilde{k}\pi\right) + 2\exp\left(i\frac{18}{11}\widetilde{k}\pi\right) + 2\exp\left(i\frac{20}{11}\widetilde{k}\pi\right)\right\}\right|^2, \tag{A6}$$

and

$$S_{13} = \left|\frac{1}{13}\left\{2 + 2\exp\left(i\frac{4}{13}\widetilde{k}\pi\right) + 2\exp\left(i\frac{6}{13}\widetilde{k}\pi\right) + 2\exp\left(i\frac{16}{13}\widetilde{k}\pi\right) + 2\exp\left(i\frac{18}{13}\widetilde{k}\pi\right) + 2\exp\left(i\frac{22}{13}\widetilde{k}\pi\right) + \exp\left(i\frac{24}{13}\widetilde{k}\pi\right)\right\}\right|^2. \tag{A7}$$

For all $\widetilde{k}$, $S_7 = 1/7$, $S_{11} = 1/11$, and $S_{13} = 1/13$. At $\widetilde{k} = 3$, $S_9 = 1/3$, and at $\widetilde{k} = 1$, 2, and 4, $S_9 = 1/9$, respectively.

APPENDIX B: RESONANCE LEVELS

The Schrödinger equation for the Hamiltonian in Eq. (1) can be written as

$$-\psi_{n-1} - \psi_{n+1} + \epsilon_n \psi_n = E\psi_n. \tag{B1}$$

It can be rewritten in terms of the transfer matrix $T(n)$,

$$\Psi_{n+1} = T(n)\Psi_n = \begin{pmatrix} \epsilon_n - E & -1 \\ 1 & 0 \end{pmatrix}\Psi_n, \tag{B2}$$

where

$$\Psi_n = \begin{pmatrix} \psi_n \\ \psi_{n-1} \end{pmatrix}. \tag{B3}$$

We set the matrix $A = \left(\begin{smallmatrix} -E & -1 \\ 1 & 0 \end{smallmatrix}\right)$ and $B = \left(\begin{smallmatrix} W-E & -1 \\ 1 & 0 \end{smallmatrix}\right)$, which corresponds to blue (A-type) sites and red (B-type) sites in Fig. 16. We consider a unit, which includes two patches and two inlaid sites [see Fig. 16(a), not including the most right red (B-type) site], so there are $s_1 + s_2 + 2$ sites. The total transfer matrix

$$T = BA^{s_2}BA^{s_1}. \tag{B4}$$

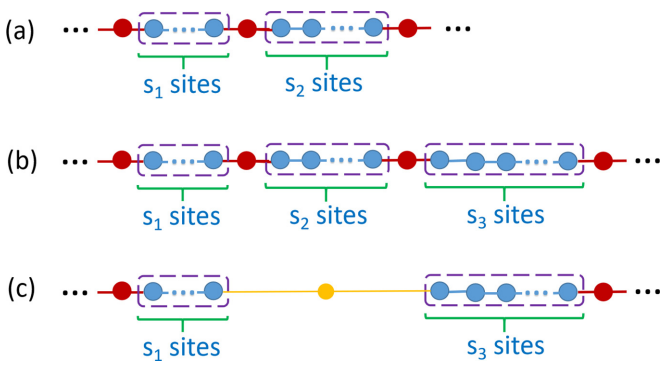

FIG. 16. The blue patches have s_j sites and inlaid single red sites link these patches.

Using the spectral decomposition method, $A = U\Lambda U^{-1}$, where $\Lambda = \left(\begin{smallmatrix} \lambda_+ & 0 \\ 0 & \lambda_- \end{smallmatrix}\right)$, and U's first and second rows are the eigenvectors of A with eigenvalues $\lambda_+ = \frac{-E+\sqrt{E^2-4}}{2}$ and $\lambda_- = \frac{-E-\sqrt{E^2-4}}{2}$, respectively. When $|E| < 2$, $\lambda_\pm = e^{\pm i\theta}$ with that $\sin\theta = \frac{\sqrt{4-E^2}}{2}$ and $\cos\theta = \frac{-E}{2}$. So

$$E = -2\cos\theta \tag{B5}$$

and

$$U = \begin{pmatrix} e^{i\theta} & 1 \\ e^{-i\theta} & 1 \end{pmatrix}, \tag{B6}$$

where $i = \sqrt{-1}$. The trace of total transfer matrix T is

$$\begin{aligned}\chi &= \mathrm{Tr}(T) = \mathrm{Tr}(BU\Lambda^{s_2}U^{-1}BU\Lambda^{s_1}U^{-1}) \\ &= a(W + 2\cos\theta)^2 + b(W + 2\cos\theta) + c,\end{aligned} \tag{B7}$$

where

$$a = \frac{1}{2\sin^2\theta}\{\cos[(s_1 - s_2)\theta] - \cos[(s_1 + s_2 + 2)\theta]\}, \tag{B8}$$

$$b = -\frac{2}{\sin^2\theta}\{\cos\theta\cos[(s_1 - s_2)\theta] - \cos[(s_1 + s_2 + 1)\theta]\}, \tag{B9}$$

and

$$c = \frac{2}{\sin^2\theta}\{\cos^2\theta\cos[(s_1 - s_2)\theta] - \cos[(s_1 + s_2)\theta]\}. \tag{B10}$$

Based on the theory of the trace map of transfer matrices [31], for allowed energies

$$|\chi(E)| \leqslant 2. \tag{B11}$$

States are extended and critical when $|\chi| < 2$ and $|\chi| = 2$, respectively.

For Eq. (B7), we consider the condition that

$$\cos[(s_1 - s_2)\theta] \approx \cos[(s_1 + s_2 + 2)\theta], \tag{B12}$$

i.e., $a \approx 0$ in Eq.(B8). We replace $\cos[(s_1 - s_2)\theta]$ by $\cos[(s_1 + s_2 + 2)\theta]$ in Eqs. (B9) and (B10), then

$$b \approx \frac{2}{\sin\theta}\sin[(s_1 + s_2 + 2)\theta] \tag{B13}$$

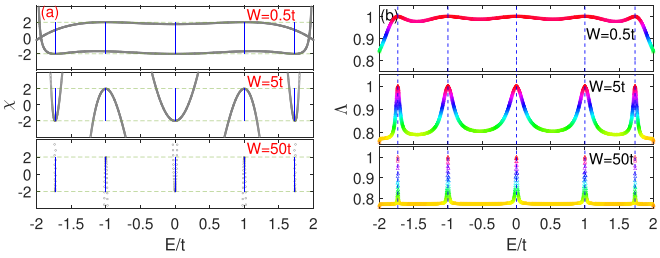

FIG. 17. (a) The trace χ and (b) RLTs Λ as functions of energies E at potential strengths $W = 0.5t, 5t$, and $50t$, respectively. Here $s_1 = 3330$ and $s_2 = 3336$. The blue vertical lines mark the positions E_M^κ with $M = |s_1 - s_2| = 6$.

and

$$c \approx 2\cos[(s_1 + s_2 + 2)\theta] - 4\cot\theta \sin[(s_1 + s_2 + 2)\theta]. \tag{B14}$$

If E in Eq. (B5) is represented by

$$E = -2\cos(\theta) = -2\cos\left(\frac{\widetilde{\kappa}\pi}{s_1 + s_2 + 2}\right), \tag{B15}$$

$\cos[(s_1 + s_2 + 2)\theta] = \pm 1$ and $\sin[(s_1 + s_2 + 2)\theta] = 0$, where $\widetilde{\kappa} = 1, 2, \ldots$. From Eqs. (B13) and (B14), we get $b \approx 0$ and $c \approx \pm 2$, so in Eq. (B7)

$$\chi \approx \pm 2, \tag{B16}$$

which is nearly independent of potential strength W. In combination with Eq. (B15), the condition in Eq. (B12) indicates

$$E \approx E_M^\kappa = -2\cos\left(\frac{\kappa\pi}{M}\right) \tag{B17}$$

with $M = |s_1 - s_2|$ and $\kappa = 1, 2, \ldots, M - 1$. The corresponding $\chi \approx \pm 2$, and states are extended or critical. If $s_1 = s_2 = s$, according to Eqs. (B12) and (B15), we get

$$E_M^\kappa = -2\cos\left(\frac{\kappa\pi}{s + 1}\right), \tag{B18}$$

which agrees with Bloch's theory.

Based on Eq. (B7), we plot χ versus energies E in Fig. 17(a) at $W = 0.5t, 5t$, and $50t$, respectively. It shows $\chi \approx \pm 2$ when E are at E_M^κ, which agrees with theoretical conclusions. The reduced local tensions (RLTs) Λ can directly characterize state localization properties [40]. Figure 17(b) shows $\Lambda \to 1$ when E are at E_M^κ, which indicates these states are extended.

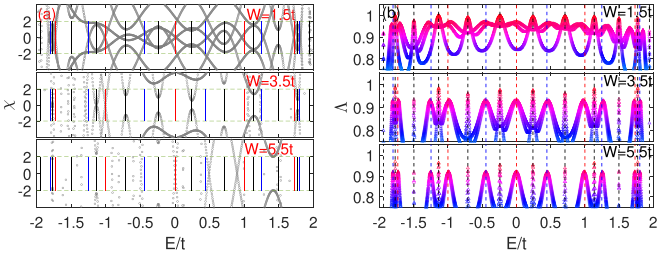

FIG. 18. (a) The trace χ and (b) RLTs Λ as functions of energies E at potential strengths $W = 1.5t, 3.5t$, and $5.5t$, respectively. Here $s_1 = 2331$, $s_2 = 2338$, and $s_3 = 2344$. The vertical lines mark the positions E_M^κ with $M = |s_1 - s_2| = 7$ (blue), $M = |s_2 - s_3| = 6$ (red), and $M = |s_1 - s_3| = 13$ (black), respectively.

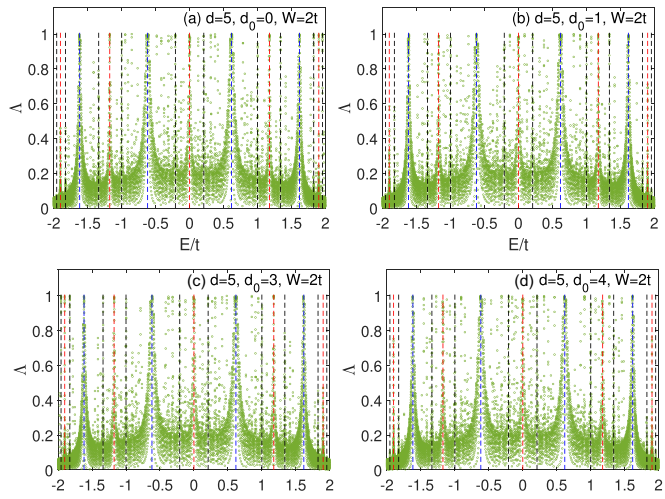

FIG. 19. At $d = 5$ and $W = 2t$, the RLTs Λ versus energies E for (a) $d_0 = 0$, (b) $d_0 = 1$, (c) $d_0 = 3$, and (d) $d_0 = 4$, respectively. The vertical dashed lines mark the positions E_M^κ with $M = 5$ (blue), $M = 10$ (blue), and $M = 15$ (black). System sizes $N = [10^4]$.

Then, we consider a unit which consists of three patches and three inlaid sites [Fig. 16(b), not including the rightmost red (B-type) site]. Using the numerically accurate renormalization scheme [32], both the sites in the intermediate patch and the intermediate inlaid sites can be renormalized into "one" inlaid site [the yellow site in Fig. 16(c)], so they can be taken as "two patches." Equation (B17) also holds but M is the size difference of the patches at two edges. Based on Eq. (B2),

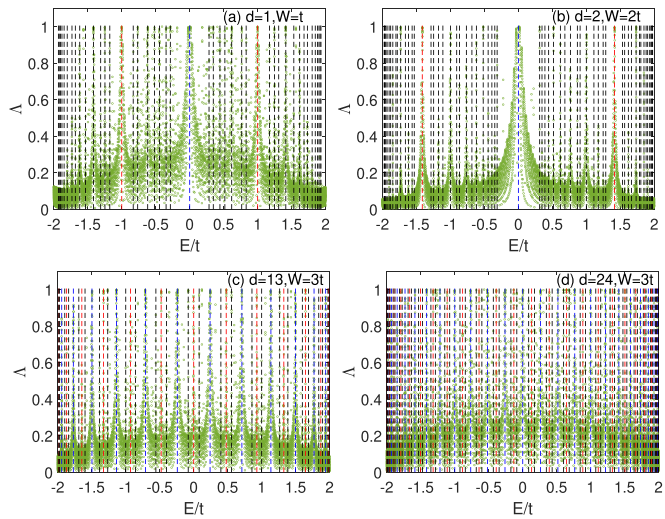

FIG. 20. At $d_0 = 2$, the RLTs Λ versus energies E for (a) $d = 1, W = t$, (b) $d = 2, W = 2t$, (c) $d = 13, W = 3t$, and (d) $d = 24, W = 3t$, respectively. The vertical dashed lines mark the positions E_M^κ. In (a), $M = 2d$ (blue), $M = 3d$ (red), and $M = 4d, 5d, \ldots, 12d$ (black), where $d = 1$; in (b), $M = d$ (blue), $M = 2d$ (red), and $M = 3d, 4d, \ldots, 10d$ (black), where $d = 2$; in (c), $M = d$ (blue), $M = 2d$ (red), and $M = 3d$ (black), where $d = 13$; in (d), $M = d$ (blue), $M = 2d$ (red), and $M = 3d$ (black), where $d = 24$. System sizes $N = [10^4]$.

we directly calculate χ. We plot χ and Λ in Figs. 18(a) and 18(b), respectively. It shows generally, χ are relatively small and Λ are relative large when E are around E_M^κ. At some E_M^κ, $\Lambda \to 1$, which indicates these states are extended. Similarly, for more patches, the results are the same, but the renormalized "inlaid" site may induce localized effects. For a few of patches (we call it a superpatch), there are states with energies E_M^κ. When these superpatches are linked together by inlaid B-type sites, the energies of whole lattices around E_M^κ may become resonance levels if they are allowed energies, and related states may be extended.

APPENDIX C: LOCAL TENSIONS AT DIFFERENT *d*

We know the reduced local tensions (RLTs) Λ can directly characterize state localization properties [40]. The larger the Λ are, the states are more extended. In Fig. 19, at $W = 2t$, we plot Λ versus energies E at $d_0 = 0, 1, 3, 4$ with $d = 5$, respectively. The Λ at $d_0 = 2$ was shown in Fig. 4. In Fig. 20, at $d_0 = 2$, we plot Λ versus E at $d = 1, 2, 13$, and 24. All the figures show Λ are relatively large when E are around E_M^κ, which indicates these states are extended (delocalized).

[1] A. Lagendijk, B. van Tiggelen, and D. Wiersma, Fifty years of Anderson localization, Phys. Today **62**(8), 24 (2009).

[2] R. N. Bhatt and S. Kettemann, Special issue "Localisation 2020": Editorial summary, Ann. Phys. **435**, 168664 (2021).

[3] P. W. Anderson, Absence of diffusion in certain random lattices, Phys. Rev. **109**, 1492 (1958).

[4] *50 Years of Anderson Localization*, edited by E. Abrahams (World Scientific, Singapore, 2010).

[5] F. Evers and A. D. Mirlin, Anderson transitions, Rev. Mod. Phys. **80**, 1355 (2008).

[6] *Aperiodic Structures in Condensed Matter: Fundamentals and Applications*, edited by E. Maciá (CRC Press, Boca Raton, FL, 2009).

[7] P. G. Harper, Single band motion of conduction electrons in a uniform magnetic field, Proc. Phys. Soc. London, Sect. A **68**, 874 (1955).

[8] S. Aubry and G. André, Analyticity breaking and Anderson localization in incommensurate lattices, Ann. Isr. Phys. Soc. **3**, 18 (1980).

[9] E. Maciá and F. Domínguez-Adame, Physical nature of critical wave functions in Fibonacci systems, Phys. Rev. Lett. **76**, 2957 (1996).

[10] C. S. Ryu, G. Y. Oh, and M. H. Lee, Extended and critical wave functions in a Thue-Morse chain, Phys. Rev. B **46**, 5162 (1992).

[11] A. Chakrabarti, S. N. Karmakar, and R. K. Moitra, Role of a new type of correlated disorder in extended electronic states in the Thue-Morse Lattice, Phys. Rev. Lett. **74**, 1403 (1995).

[12] *Quasicrystals: Fundamentals and Applications*, edited by E. Maciá (CRC Press, Boca Raton, FL, 2021).

[13] A. Brezini and N. Zekri, Overview on some aspects of the theory of localization, Phys. Status Solidi B **169**, 253 (1992).

[14] J. B. Pendry, Quasi-extended electron states in strongly disordered systems, J. Phys. C: Solid State Phys. **20**, 733 (1987).

[15] J. B. Pendry, Symmetry and transport of waves in one-dimensional disordered systems, Adv. Phys. **43**, 461 (1994).

[16] D. Leykam, A. Andreanov, and S. Flach, Artificial flat band systems: From lattice models to experiments, Adv. Phys. **3**, 1473052 (2018).

[17] M. Goda, S. Nishino, and H. Matsuda, Inverse Anderson transition caused by flat bands, Phys. Rev. Lett. **96**, 126401 (2006).

[18] D. H. Dunlap, H-L. Wu, and P. W. Phillips, Absence of localization in a random-dimer model, Phys. Rev. Lett. **65**, 88 (1990).

[19] D. Giri, P. K. Datta, and K. Kundu, Tuning of resonances in the generalized random trimer model, Phys. Rev. B **48**, 14113 (1993).

[20] R. Farchioni and G. Grosso, Electronic transport for random dimer-trimer model Hamiltonians, Phys. Rev. B **56**, 1170 (1997).

[21] S. N. Evangelou and E. N. Economou, Reflectionless modes in chains with large-size homogeneous impurities, J. Phys. A: Math. Gen. **26**, 2803 (1993).

[22] D. López-González and M. I. Molina, Transport of localized and extended excitations in chains embedded with randomly distributed linear and nonlinear n-mers, Phys. Rev. E **93**, 032205 (2016).

[23] F. M. Izrailev, T. Kottos, and G. P. Tsironis, Hamiltonian map approach to resonant states in paired correlated binary alloys, Phys. Rev. B **52**, 3274 (1995).

[24] D. A. Bykov, E. A. Bezus, A. A. Morozov, V. V. Podlipnov, and L. L. Doskolovich, Optical properties of guided-mode resonant gratings with linearly varying period, Phys. Rev. A **106**, 053524 (2022).

[25] D. S. Citrin, Quadratic superlattices: A type of nonperiodic lattice with extended states, Phys. Rev. B **107**, 125150 (2023).

[26] D. Kulkarni, D. Schmidt, and S.-K. Tsui, Eigenvalues of tridiagonal pseudo-Toeplitz matrices, Linear Algebra Appl. **297**, 63 (1999).

[27] E. J. Torres-Herrera, J. A. Méndez-Bermúdez, and L. F. Santos, Level repulsion and dynamics in the finite one-dimensional Anderson model, Phys. Rev. E **100**, 022142 (2019).

[28] Zh. Cheng, R. Savit, and R. Merlin, Structure and electronic properties of Thue-Morse lattices, Phys. Rev. B **37**, 4375 (1988).

[29] G. Y. Oh and M. H. Lee, Band-structural and Fourier-spectral properties of one-dimensional generalized Fibonacci lattices, Phys. Rev. B **48**, 12465 (1993).

[30] R. Merlin, Structural and electronic properties of nonperiodic superlattices, IEEE J. Quantum Electron. **24**, 1791 (1988).

[31] M. Kohmoto, L. P. Kadanoff, and C. Tang, Localization problem in one dimension: Mapping and escape, Phys. Rev. Lett. **50**, 1870 (1983).

[32] R. Farchioni, G. Grosso, and G. P. Parravicini, Electronic structure in incommensurate potentials obtained using a numerically accurate renormalization scheme, Phys. Rev. B **45**, 6383 (1992).

[33] A. D. Mirlin, Statistics of energy levels and eigenfunctions in disordered systems, Phys. Rep. **326**, 259 (2000).

[34] P. Carpena, V. Gasparian, and M. Ortuño, Energy spectra and level statistics of Fibonacci and Thue-Morse chains, Phys. Rev. B **51**, 12813 (1995).

[35] T. A. Brody, J. Flores, J. B. French, P. A. Mello, A. Pandey, and S. S. M. Wong, Random-matrix physics: Spectrum and strength fluctuations, Rev. Mod. Phys. **53**, 385 (1981).

[36] S. Das Sarma, S. He, and X. C. Xie, Mobility edge in a model one-dimensional potential, Phys. Rev. Lett. **61**, 2144 (1988).

[37] S. S. de Albuquerque, F. A. B. F. de Moura, and M. L. Lyra, Resonant localized states and quantum percolation on random chains with power-law-diluted long-range couplings, J. Phys.: Condens. Matter **24**, 205401 (2012).

[38] B. I. Shklovskii, B. Shapiro, B. R. Sears, P. Lambrianides, and H. B. Shore, Statistics of spectra of disordered systems near the metal-insulator transition, Phys. Rev. B **47**, 11487 (1993).

[39] P. Carpena, P. Bernaola-Galván, and P. Ch. Ivanov, New class of level statistics in correlated disordered chains, Phys. Rev. Lett. **93**, 176804 (2004).

[40] E. V. F. de Aragão, D. Moreno, S. Battaglia, G. L. Bendazzoli, S. Evangelisti, T. Leininger, N. Suaud, and J. A. Berger, A simple position operator for periodic systems, Phys. Rev. B **99**, 205144 (2019).

[41] S. Evangelisti, F. Abu-Shoga, C. Angeli, G. L. Bendazzoli, and J. A. Berge, Unique one-body position operator for periodic systems, Phys. Rev. B **105**, 235201 (2022).

[42] Y. Chen and L. Gong, Statistical properties related to angle variables in Hamiltonian map approach for one-dimensional tight-binding models with localization, Eur. Phys. J. B **96**, 8 (2023).

[43] Y. Tao, Anderson localization in one-dimensional systems signified by localization tensor, Phys. Lett. A **455**, 128517 (2022).

[44] B. Kramer and A. MacKinnon, Localization theory and experiment, Rep. Prog. Phys. **56**, 1469 (1993).

[45] I. Varga, J. Pipek, and B. Vasvári, Power-law localization at the metal-insulator transition by a quasiperiodic potential in one dimension, Phys. Rev. B **46**, 4978 (1992).

[46] A. Ahmed, A. Ramachandran, I. M. Khaymovich, and A. Sharma, Flat band based multifractality in the all-band-flat diamond chain, Phys. Rev. B **106**, 205119 (2022).